Advances in Science and Technology Research Journal

Advances in Science and Technology Research Journal 2023, 17(3), 170–183
https://doi.org/10.12913/22998624/166101
ISSN 2299-8624, License CC-BY 4.0

Received: 2023.03.27
Accepted: 2023.05.14
Published: 2023.06.01

Supported by 2D and 3D Imaging Methods Investigation of the Influence of Fiber Orientation on the Mechanical Properties of the Composites Reinforced with Fibers in a Polymer Matrix

Robert Saraczyn[1*], Martyna Deroszewska[1], Tomasz Kowaluk[2], Emilia Skołek[3], Witold Rządkowski[4], Dawid Myszka[1]

[1] Faculty of Mechanical and Industrial Engineering, Warsaw University of Technology, Pl. Politechniki 1, 00-665 Warsaw, Poland
[2] Faculty of Mechatronics, Warsaw University of Technology, Pl. Politechniki 1, 00-665 Warsaw,, Poland
[3] Faculty of Materials Science and Engineering, Pl. Politechniki 1, 00-665 Warsaw,, Poland
[4] Faculty of Power and Aeronautical Engineering, Pl. Politechniki 1, 00-665 Warsaw,, Poland
* Corresponding author's e-mail: robert.saraczyn.dokt@pw.edu.pl

ABSTRACT

The aim of this study was to examine the behavior of the carbon fiber reinforced polymer (CFRP) composites depending on the fiber orientation and to understand the influence of microstructural discontinuities on mechanical properties. For the tests 210 gsm prepreg composite and 200 gsm carbon fabric with polymer matrix have been used. Samples were structured and later examined according to the ASTM-D3039 and ASTM-D3878 (equivalents are ISO 20975, ISO 527-4 and ISO 527-5). Accordingly, to the number of layers, three ways of the fibers arranging in relation to the applied force were used. Mechanical properties were determined in a static tensile test. The results of imaging studies, which included analyzes of Digital Image Correlation, Computed Tomography and Scanning Electron Microscopy, showed structural discontinuities, specific stress distribution and propagation of stresses depending on the production technology, which were correlated with the obtained strength results. The source of the gradual development of the degradation of the composite structure was observed in local microdamages and microcracks. As a result of a sub-critical crack growth within the resin matrix material, the defects are subject to a complex, multi-axial stress field on the micro-scale, even if the globally applied force is axial**.** Samples in which the load was applied along the axis of the fibers behave like an elastic material, while samples, where the force is applied at an angle to the axis of the fibers, tend to behave like an elastic-plastic material.

Keywords: image analysis, fiber orientation, tensile test, CFRP, computed tomography, microscopy

INTRODUCTION

Fiber reinforced polymer (FRP) composites are applicable in every field of our daily life [1] and their use is steadily increasing due to the dissemination of technology and the fall in material prices. The reason FRP are gaining importance all the time is their incredibly good mechanical strength to weight ratio and corrosion resistance [2, 3]. Additionally, thanks to the use of diverse types of fibers and matrix material, the desired properties can be obtained. Mechanical properties of the composite are dependent on processing technique, an adequate combination of reinforcement [4], percolation of structure elements [5], fiber volume or weight fraction, fiber type and density, matrix density and viscosity etc. [1, 6].

Carbon fiber belongs to the group of synthetic fibers that do not occur naturally but are formed as a result of chemical processes from synthetic polymers, i.e., substances with a very high molecular weight, consisting of repeatedly replicated units called mers. These are fibers with carbon threads with a diameter of about 5 to 10 micrometers,

consisting primarily of carbon atoms. Carbon fibers are characterized by good heat and chemical resistance compared to other fibers – both natural and synthetic. The main advantages of carbon fibers are high stiffness, low density, fatigue resistance, good electrical and thermal conductivity. In addition, these fibers have the ability to damp vibrations and have low X-ray absorption [7-9].

When producing composite structures, it is particularly important to obtain the desired mechanical properties without oversizing the structure. This is controlled by the use of an appropriate number of layers for a given case [4, 10]. The texture and morphology of the carbon fibers surface depend greatly on the surface modification conditions [11].

FRP composites are manufactured using a variety of techniques. This study covers two production technologies:

- pre-impregnated combination of fibers and uncured resin, which is activated by the temperature [12]
- vacuum bag molding with assistance of the hand lay-up technique [13]

At the stage of designing composites, depending on the loads they will be exposed to, it is possible to control their strength properties in various planes by controlling the sequence of lay-ups [14, 15, 16]. The highest tensile strength values are obtained when the stresses occur along the fiber direction [17]. When the direction of the tensile stresses deviates from the direction of the fibers, there are more and more stress components perpendicular to the axis of the fibers, which increases the proportion of the matrix in the load transmission and, finally, the strength of the entire composite decreases.

Tensile tests are conducted on purpose to determine values of strength and modulus [4, 18], which will be used to determine the necessary technology to make a product with the desired properties for the environment in which the product will work. The examination of cracks initiation and their propagation may translate into an improvement in the mechanical properties of the created composites [19, 20].

METHODOLOGY

In this work, the impact of irregular fiber breaking of carbon fiber reinforced polymer (CFRP) on the whole structure is investigated as well as the effect of different fiber orientations on tensile strength.

Two different composites were produced in two technologies, using reinforcement and matrix with similar strength parameters. The following research methods were used in the composite sample testing process: static tensile test, digital image correlation (DIC), scanning electron microscopy (SEM) and computed tomography (CT). The terminology used in these research descriptions is taken from ASTM-D3878 [21].

MATERIALS, TECHNOLOGIES AND LAYUP

To understand the behavior of the composite materials depending on the fiber orientation, different layups have been presented as well as two different lamination technologies, for comparison. The dimensions of the samples are shown in Figure 1. The number of plies comes indirectly from the ASTM D3039 as the thickness of the middle section should have a dimension of 1 mm [22].

The composites used in the study were made in two technologies, which allowed for the determination of deviations related to the production process and the improvement of the quality of the tests conducted. Due to the different thicknesses of the laminate layers, in the case of these two technologies, a different number of layers was placed. The thickness, however, remained the same, in line with the standards.

The first technology for preparing samples was a pre-impregnated combination of fibers and uncured resin, activated by the temperature. To perform tests, 210 gsm out-of-autoclave (OOA) XPREG XC110 acquired from [23] has been used. This is a pre-preg system based on Pyrofil TR30S 3K carbon fabric with a 2×2 twill weave with fibers oriented at 0 and 90 and pre-impregnated

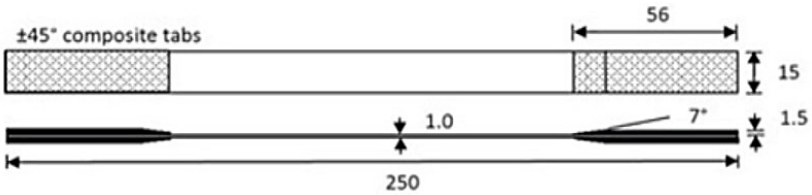

Fig. 1. Dimensions of the sample (in mm) according to ASTM D3039 [22]

with an epoxy resin system in the b-stage. Areal weight per ply including resin is 362 g/m^2, while resin weight in the composite is 42%. Samples of standard dimensions were cut from the pre-impregnated fabric, the appropriate number of layers were laid, and then prepared for hardening under vacuum and heating in the furnace. The annealing cycle with the curing temperature of 132°C (for 4 hours) was consistent with the product data sheet attached [23] and it included increasing the temperature of the process in cycles.

The second technology for preparing samples was vacuum bag molding with the assistance of the hand lay-up technique [24]. For the production of samples using this method, a carbon fabric with a grammage of 200 g/m^2 and a polymer matrix, which was a mixture of bisphenol resin and hardener, were used. The resin L285 MGS and the hardener number 285, acquired from Havel Composites, were selected for the fabric to match the properties of the XPREG XC110 composite. Resin and hardener were mixed in the ratio of 10:4. Areal weight per ply including resin is 362 g/m^2, while resin weight in the composite is 44,8%. Samples of standard dimensions were cut from the carbon cloth sheet, the appropriate number of layers were laid, and then prepared for hardening under vacuum.

Due to the fact that the fabric in the process of manual lamination with the use of brushes and rollers tends to change its position, fiber stretching and fraying, an allowance for finishing treatment was used. The samples that are tested must be standardized, i.e., their dimensions are strictly defined. In order to increase the dimensional accuracy, the laminated products were cut on a numerically controlled milling plotter. For the needs of this machining, a simple program was created to control the machine tool spindle.

Composite materials were made to be assessed on a testing machine. In order to reduce local stresses introduced by the jaws of the apparatus, fiberglass mounting brackets have been laminated as shown in Figure 2. Their dimensions and the method of mounting them on the samples comes directly from the standards. The first step was to grind the samples corresponding to the length of the handles on both sides. The purpose of this treatment was to provide a greater surface roughness so that the materials would properly bond together. For the purpose of making the overlays, the glass fabric was cut into fragments of appropriate dimensions. An aluminum plate on which the operation was performed was appropriately prepared. Then, a mixture of resin and hardener was prepared. L285 MGS resin and 285 hardener in the ratio of 10:4 were used for this purpose. Handles have been laminated on both sides of the samples. The plate was covered with a peel-off fabric, flexible foil and a vacuum bag secured with butyl tape and connected by a valve to a vacuum pump. The process air was sucked off due to the vacuum effect.

Research instrumentation

The first step of sample preparation for testing on a testing machine was to laminate the glass fiber reinforced polymer (GFRP) tabs on both sides of the sample in accordance with the ASTM D3039 standard.

Tests were performed on Instron 8516 Testing System acquired from [25] and shown in Figure 4. The samples were stretched at a speed of 0.1 mm/s. Extensometer has not been used. The data recorded by the machine are time, position [mm] and load [N]. The stress and strain were obtained as a result of the following calculations:

$$\sigma = \frac{\mathrm{F}}{d \times n \times s} \tag{1}$$

where: σ – stress at current time step [MPa], F – load at current time step [N], d – single layer thickness for a given sample [mm], n – the number of layers used in a given sample, s – cross-section of the center of the sample [mm].

Table 1. L285 MGS resin and 285 hardener specification

Parameter	L 285 MGS Resin	285 Hardener
Density (g/cm^3 / 25 °C)	1.18-1.23	0.94-0.97
Viscosity (mP/s / 25 °C)	600-900	50-100
Epoxy number (-)	0.59-0.65	-
Amine number (mg KOH/G)	-	480-550

Table 2. Tested samples and their characteristic

Samples	Technology	Number of plies	Layup
1-3	1	4	(0;0;0;…)
4-6	1	4	(45;45;45;…)
7-9	1	4	(0;45;0;45;0;45;…)
10-12	2	8	(0;0;0;…)
13-15	2	8	(45;45;45;…)
16-18	2	8	(0;45;0;45;0;45;…)

a) b)

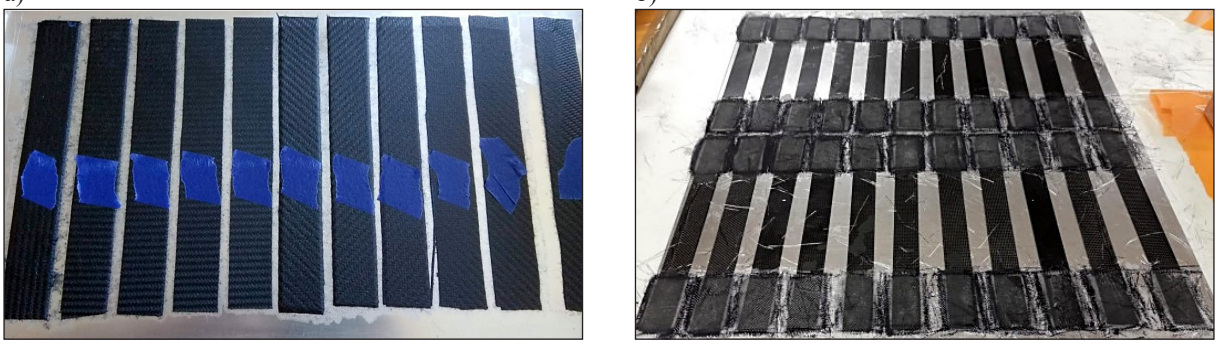

Fig. 2. Samples after the lamination process – a) without handles, b) with handles

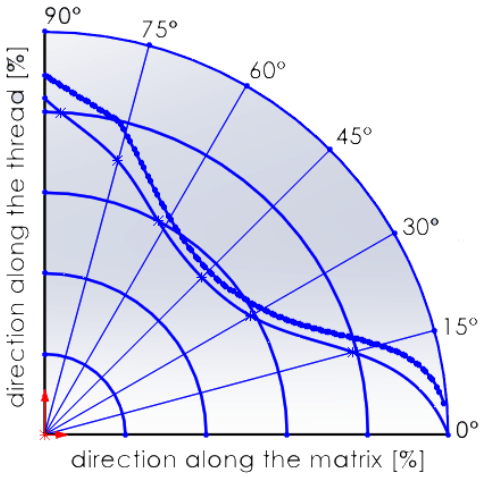

Fig. 3. Changes in the strength indexes of the fabric-reinforced composite depending on the angle of the reinforcement arrangement in relation to the load direction [17]

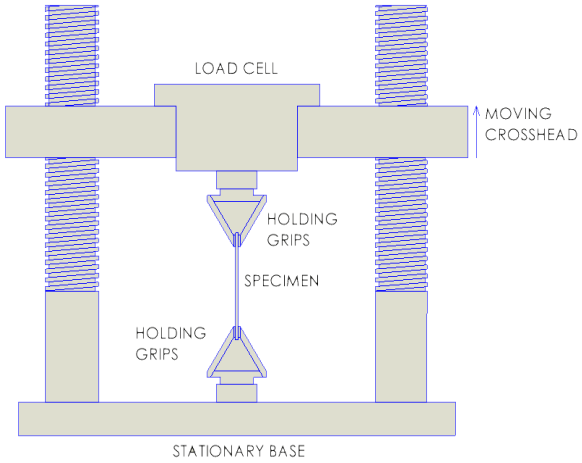

Fig. 4. Tensile testing system setup. Schematic view of the machine

$$\varepsilon = \frac{\lim_{L \to 0} \frac{\Delta L}{L}}{l} \tag{2}$$

where: ε – strain at current time step [%], L – displacement at current time step [mm], l – length of the given sample being stretched without GFRP tabs.

Digital Image Correlation (DIC) is a research method that measures the entire recorded area and analyzes the parameters in each direction. It allows, for example, to observe the change in the stiffness of the composite sheathing at the point of changing the arrangement of the layers or to notice the heterogeneity of the theoretically homogeneous material. In the DIC system, the purpose of image analysis is to create a three-dimensional map of deformation using photos of the undeformed and deformed samples. The main parameter for examining an image is grayscale. After removing the colors and applying randomly distributed spots on the surface of the body, an image that is easy to analyze by an algorithm is obtained. Based on the analysis of the intensity of the light beam reflected from the surface in the state before and after the load is applied, non-contact measurement of changes in the displacement state components is made.

The image was captured during the tensile strength test. In order to adapt the tested composites to the static tensile test using digital image correlation, a texture in the form of two layers of white, matte spray paint was applied to their surface. Then, black spots were randomly placed on the texture. During the test, the dyed side of the samples was recorded, and the deformations were read on the basis of changes in the position of points between the frames.

Figure 5 shows a diagram of the method of imaging with the use of two cameras (CCD1 and CCD2), where the alpha angle corresponds to the

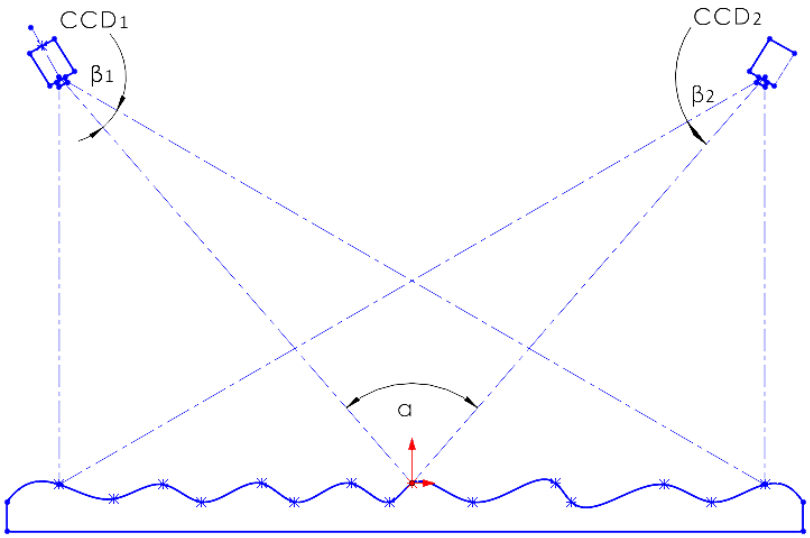

Fig. 5. Scheme of 3D measurement using two cameras

value of the angle between the middle beams of light received by the cameras, and the beta angles between the middle beam and the beam of the edge of the working field (observation field).

A Scanning Electron Microscope (SEM) was used to test samples of composite materials reinforced with fibers in a polymer matrix [26]. The wavelength of accelerated electrons in the case of SEM is much smaller than the wavelength of visible light, which allows for much higher resolution compared to light microscopy. The condition for the use of electron microscopy is a vacuum of at least 10^{-4} Pa.

The research was carried out on a Hitachi Scanning Electron Microscope S3500N. The samples were cut to the dimensions of the table in the working chamber of the device – 20×20 mm. In order to improve the imaging of the produced composites, the samples were sprayed with MM59 manganese brass alloy [27, 28]. Secondary electron detector has been used. Accelerating voltage used – 5 kV.

An additional batch of samples was prepared and tested without shredding – for comparison. The remaining samples (1-18, Table 2) were broken on the machine and then they were cut out.

Computed tomography (CT), thanks to the use of X-rays, allows to reconstruct the interior of the tested product. The tomograph takes X-rays of detail from many different angles and then joins them together to form a 3D model. This is because the cone-shaped X-ray tube generates an X-ray beam, which allows the overexposed object to be projected onto a digital detector. The tested detail rotates around its axis by a given angle, while a digital photo is taken in various positions. Based on the obtained data, the software reconstructs the image [29].

A Metrotom 800 tomograph was used to test the prepared composite materials. It is equipped with an X-ray tube with a maximum voltage of 130 kV. The detector allows to obtain an image with a resolution of 1920×1536 pixels. Measurements with this device are carried out in two stages - scanning and data analysis. The time spent analyzing the data depends on the assumptions about the information obtained. For the analysis of the samples made, a standard report was generated in the form of a series of sections from three directions. The scanning process of the samples took 180 minutes in both series of the CT tests (before and after conducting mechanical tests). Used voltage – 80 kV, acquired images – 1000, nominal resolution – 7 µm.

RESULTS AND DISCUSSION

The results were analyzed in terms of the strength properties of the material, depending on the orientation of the fibers, the correlation of technological defects with the results of strength tests, including structural discontinuities for the weakening of the entire structure. The focus was also on the heterogeneous distribution of stresses and strains during the tensile test. Graphical data is presented in Table 3 and Table 4, corresponding to sample numbers 1-9 and 10-18. Input data,

linked with the used machinery, for obtaining results have been described before. Maximum stress is the highest stress value recorded, while stress at failure is the stress value recorded when the sample breaks.

For the tested group of samples, the standard deviation and standard error were calculated according to the following formulas:

$$\sigma = \sqrt{E\left(\left(X - E(X)\right)^2\right.} \tag{3}$$

where: σ – standard deviation, $E(X)$ – expected value of X,

$$\sigma_\mu = \frac{\sigma}{\sqrt{N}} \tag{4}$$

where: σ_μ – standard error, N – number of tested samples.

The obtained results are shown in Figures 6 and 7 and correlated with the previously created model shown in Figure 3. A peak value for every sample occurs just before breaking and is related to skin failure, when some of the fibers reach their tensile strength limit. Interesting behavior is observed for samples 10, 13 and 15 in which stress at failure value is different from the maximum obtained stress value and occurs distinctly before the breaking of samples – shown in Figure 7. This usually means that necking is occurring. The sample reduces its cross-section, which is not included in the classical formula. While the stress on the neck may continue to increase, reducing the size means the force probably decrease. This indicates some plastic properties of the material.

When calculating the standard deviation and standard error the following values were obtained: standard deviation – 43.77 MPa, standard error – 10.31 MPa. This means that the values presented in Table 3, Table 4 and Table 5 may differ from the actual values by +/- 10.31 MPa.

In the tensile strength test results, higher tensile strength values and greater repeatability of the results for the samples made in the first technology can be observed. Due to the fact that the strength values are higher and the percentage value of elongation, especially for samples 4, 5 and 6 in relation to samples 13, 14 and 15 is significantly higher, it should be stated that the first method is more effective. Therefore, one should look at the microstructure of the material to determine the cause of this state.

The results were processed and analyzed in the Istra 4D software. Engineering Tangential

Table 3. Results of tensile strength test for samples 1-9 (pre-impregnated CFRP)

Sample	Stress at failure [MPa]	Strain at failure [%]	Maximum stress [MPa]	Layup
1	1274.0	2.73	1274.0	(0;0;0;…)
2	1280.6	2.74	1280.6	(0;0;0;…)
3	1212.3	2.56	1212.3	(0;0;0;…)
4	246.2	16.00	246.2	(45;45;45;…)
5	249.1	14.88	249.1	(45;45;45;…)
6	258.7	14.65	258.7	(45;45;45;…)
7	667.2	1.62	667.2	(0;45;0;45;0;45;…)
8	685.5	1.66	685.5	(0;45;0;45;0;45;…)
9	792.4	1.41	792.4	(0;45;0;45;0;45;…)

Table 4. Results of tensile strength test for samples 10-18 (hand lay-up CFRP)

Sample	Stress at failure [MPa]	Strain at failure [%]	Maximum stress [MPa]	Layup
10	856.7	1.58	1114.1	(0;0;0;…)
11	934.7	1.60	934.7	(0;0;0;…)
12	838.3	1.25	838.3	(0;0;0;…)
13	229.9	6.91	272.5	(45;45;45;…)
14	223.2	7.46	223.2	(45;45;45;…)
15	305.7	3.90	301.9	(45;45;45;…)
16	567.3	1.17	567.3	(0;45;0;45;0;45;…)
17	621.0	1.31	621.0	(0;45;0;45;0;45;…)
18	570.7	1.60	570.7	(0;45;0;45;0;45;…)

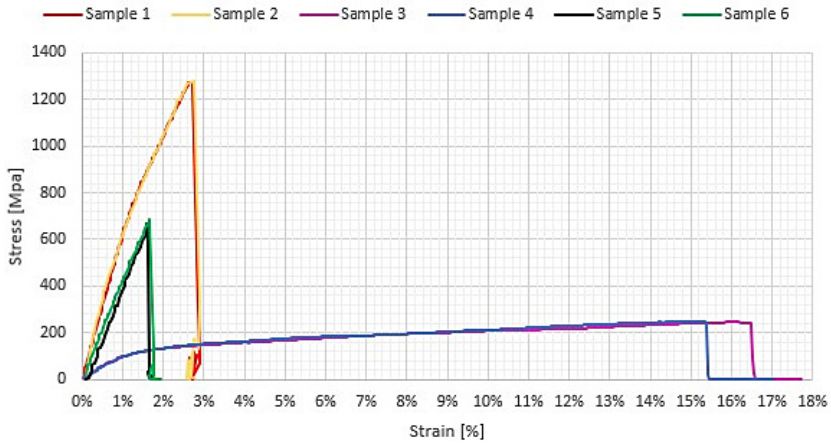

Fig. 6. Stress-strain chart for CFRP samples made in pre-impregnated combination of fibers and uncured resin, activated by temperature technology

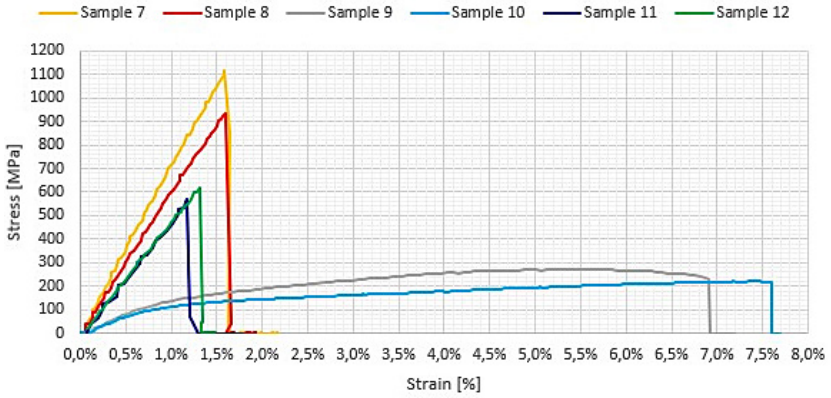

Fig. 7. Stress-strain chart for CFRP samples made in vacuum bag molding with assistance of the hand lay-up technique

Table 5. Average results of tensile strength test by category

Samples	Technology	Number of plies	Layup	Average maxium stress [MPa]
1-3	1	4	(0;0;0;…)	1255.6
4-6	1	4	(45;45;45;…)	251.3
7-9	1	4	(0;45;0;45;0;45;…)	715.0
10-12	2	8	(0;0;0;…)	962.4
13-15	2	8	(45;45;45;…)	265.9
16-18	2	8	(0;45;0;45;0;45;…)	586.3

Strains, presented on the y-axis, are shown along the samples. The x-axis shows the distance from the leftmost point of the sample, wherein extreme values on the x-axis should be ignored due to the technical capabilities of cameras that do not capture all sample points. Results are shown in Figures 8–11.

The samples made in two technologies, for the corresponding angular arrangement of the layers, were compared – number 2 and 3 to number 11 and 12. The presented photos show the accumulation of stresses just before breaking the sample during the tensile test.

A significant difference should be noted in the areas of highest stress culmination. For the pre-impregnated technology, samples 2 and 3, these are evenly distributed in the central part of the sample and reach the highest values at the point where the glass fiber handles are attached. For the samples 11 and 12, made in the hand lay-up technology, it can be observed that the stresses transferred in the central part have different

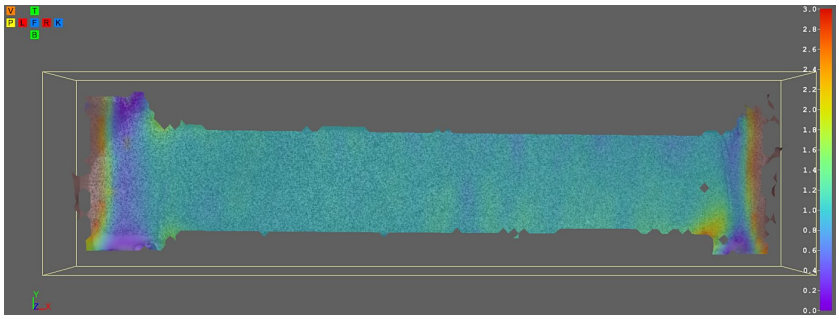

Fig. 8. Engineering Tangential Strain (strain [%] in the distance [mm] function) at a given point – sample number 2

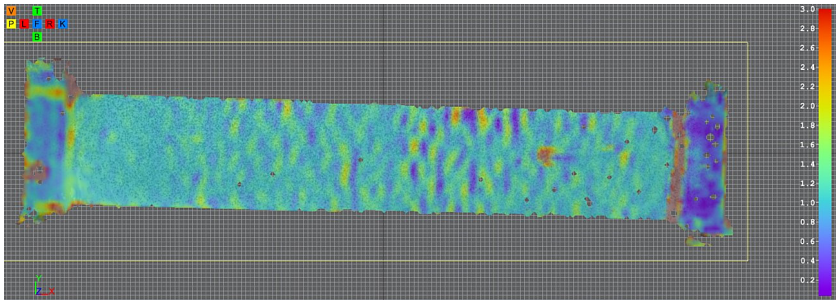

Fig. 9. Engineering Tangential Strain (strain [%] in the distance [mm] function) at a given point – sample number 3

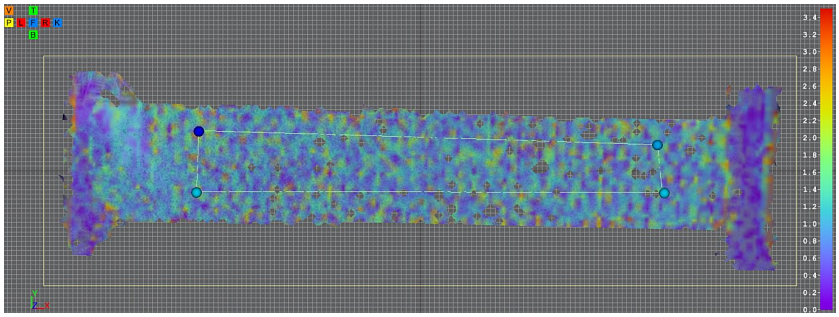

Fig. 10. Engineering Tangential Strain (strain [%] in the distance [mm] function) at a given point – sample number 11

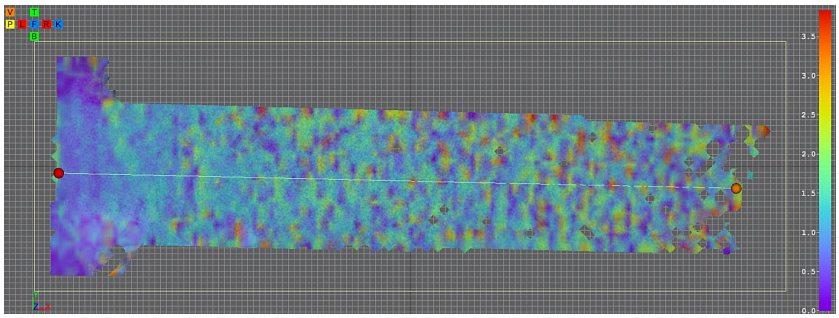

Fig. 11. Engineering Tangential Strain (strain [%] in the distance [mm] function) at a given point – sample number 12

values, the peaks of which are dispersed along the entire length. The similarity is the fact that high values are observed in the places where the handles are mounted.

What is particularly significant from the point of view of the analysis of the correlation of the strength values with the results obtained with the use of imaging techniques is the fact that in the

event of the appearance of structural discontinuities resulting from technological defects in the sample production process, unavoidable for the manual method, subsequent strands of fibers protect each other while weakening the entire structure. This means that the maximum stress values that the material is able to transfer are dissipated.

During fatigue loading, initiated and then progressing cracks in the matrix cause a simultaneous increase in the stresses transmitted by the fibers. The occurrence of cracks in individual carbon fibers causes the surrounding fibers to break sequentially, which results in premature failure of the entire sheets [30].

When analyzing the results of imaging made with the use of SEM, differences in the surface structure of the samples should be noted, where it is possible to notice discontinuities in the matrix but also discontinuities in the thread structure, resulting from delamination due to the filtration of the fibrous structure with the polymer mixture [31]. The samples were dusted to increase the conductivity, thanks to which the structural discontinuities can be observed in the image and a comparison can be made. Discontinuities cannot be quantified, but a correlation between homogeneities can be referred to the results shown in Table 3 and Table 4. Figures 12 and 13 present composites made in two technologies, where the fibers are arranged at different angles to the tensile force.

The distribution of the structural discontinuities is random, however quite densely packed, which can be correlated with juxtaposition of Figure 12b with Figure 10, since the solid structure in the stress-affected area is the protection point for the weakened areas.

The plane that was observed in the CT examination for Figures 15, 16, 17 and 18 is indicated in Figure 14. Figures 17 and 18 show where the samples broke during the static tensile test. The same place is shown (for sample number 2 and sample number 11, respectively), but it is presented in a mirror image. Figures 19 and 20 show where the sample breaks perpendicularly to that spot.

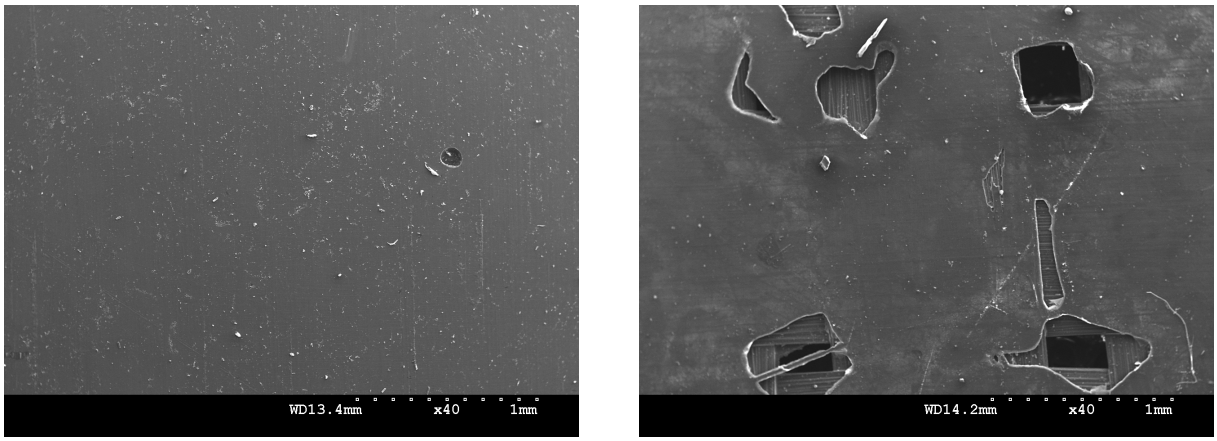

Fig. 12. View of the structure – samples with fibers at 0 degrees a) sample no. 2 b) sample no. 11

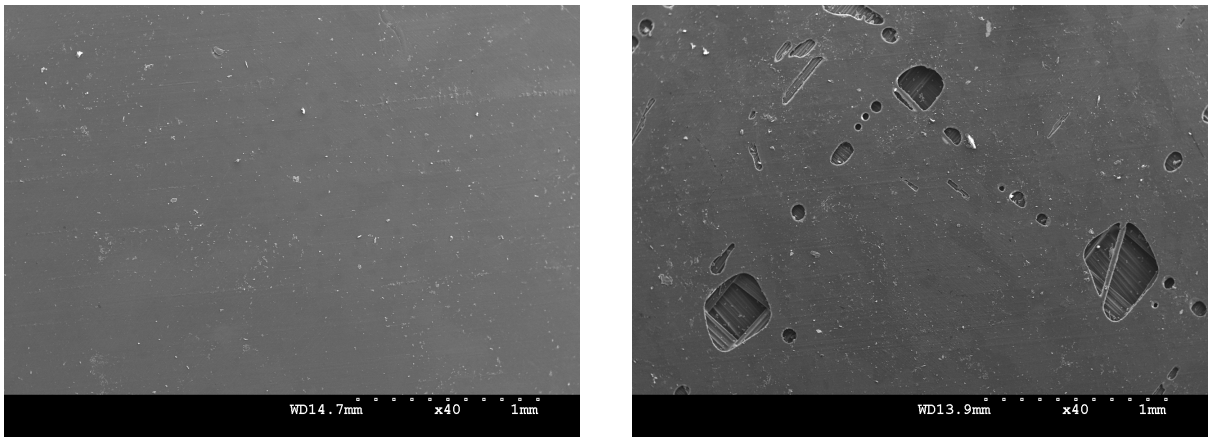

Fig. 13. View of the structure – samples with fibers at 45 degrees a) sample no. 5 b) sample no. 14

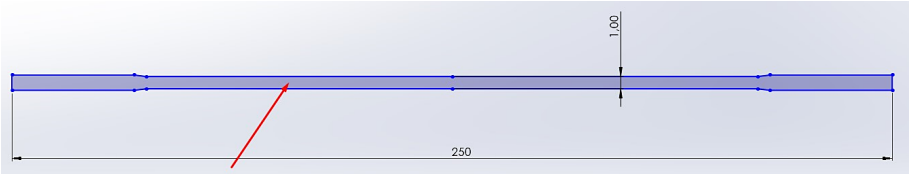

Fig. 14. Plane observed in CT examination for Figures 15, 16, 17 and 18

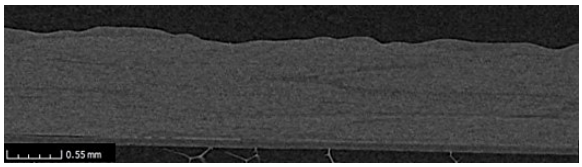

Fig. 15. View of the structure before conducting a mechanical test – sample number 2

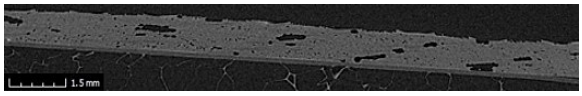

Fig. 16. View of the structure before conducting a mechanical test – sample number 11

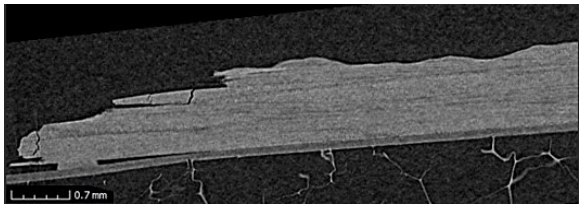

Fig. 17. View of the structure after conducting a mechanical test – sample number 2

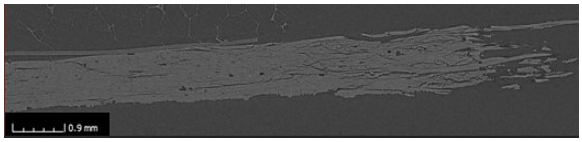

Fig. 18. View of the structure after conducting a mechanical test – sample number 11

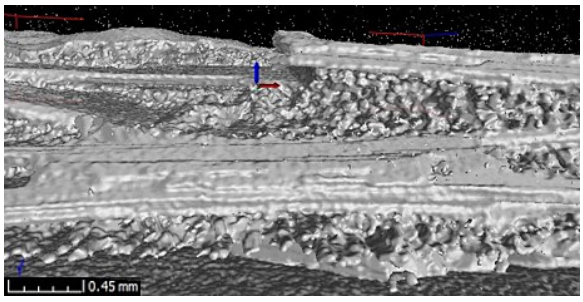

Fig. 19. View of the structure after conducting a mechanical test – sample number 2

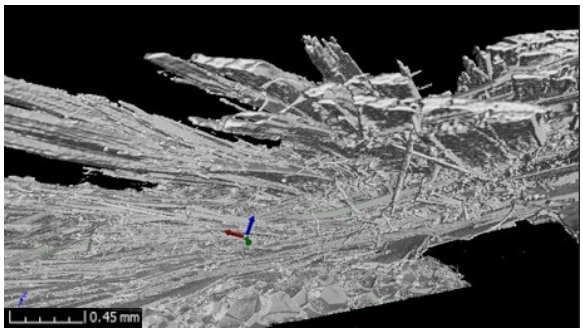

Fig. 20. View of the structure after conducting a mechanical test – sample number 11

For imaging performed with the use of computed tomography, a significant difference can be noticed in the porosity of the material – in the pre-impregnated composite (Fig. 15) it is practically absent at the resolution level of the apparatus. Figure 16 shows numerous unfilled areas of the structure along the entire cross-section of the sample – so not only on the surface.

In the case of samples made in the manual lamination technology, on the example of Figure 20, much greater delamination of individual layers and fibers within these layers can be observed, compared to Figure 19. The location of the fracture of the samples indicates that the fracture mechanics differed from each other for the tested objects.

Observation of the images obtained from the tomograph apparatus allows to relate to behavior in the field of fracture mechanics. In Figures 17 and 18 the propagation of deformations into the material is visible. In both cases, one can see that the structure of the outermost layer has undergone significant deformation, where the thread has undergone a wavy effect due to the tensile force. An interesting phenomenon, however, is the propagation of deformations and cracks into the material. In the case of the first technology of making samples, it can be observed that the structure is deformed into the material, but the layers did not

separate from each other. In the case of the second technology, a more stochastic delamination of individual layers may be noticed as well as the propagation of cracks into the material. This indicates mutual protection of the entire structure while subjecting it to the loads.

CFRP epoxy composites may contain micropores or micro-cracks from the manufacturing process, e.g., caused by insufficient laboratory equipment to conduct optimal methods or relaxation of residual stresses [32]. These defects are furthermost probably subject to a complex, multiaxial stress field on the micro-scale even if the globally applied force is axial. To understand the behavior of fracture mechanics for composite materials, they should be tested and compared to the metal components while excessive loading and manufacturing inaccuracies may invoke a process analogous to fatigue in metal components resulting in the ultimate failure of the component [33]. Conducted research proved that this mechanism is a result of sub-critical crack growth within the resin matrix material.

The behavior of small and short cracks in CFRP possibly can be drawn from testing macroscale components and comparing the observed fatigue crack growth behavior with models based on Paris-type law and associated threshold or the Hartman-Schjive approach [32].

The results show that the uniformly stretched cuboidal sample undergoes transverse deformation, i.e., warping.

For two lamination technologies it is possible, based on the observation of samples after breaking, determine how the composite material has been damaged, preventing further load transfer by this particular structure. For pre-impregnates, the fracture mechanics is comprised of the layer fracture, where the transverse fractures of the individual laminate layers arise as a result of combining the fracture of the boundary layer with the matrix microcracks [17], which is illustrated in Figures 21 and 22. The high modulus of CFRP composites transfer fatigue stresses along the fibers. Propagated transverse cracks induce local damage concentrations [30].

Analyzing Figure 20 it can be observed that for the manual lamination technology, a transverse breakage of the fibers occurs, which results from the fact that the destructive longitudinal deformation of the fibers is smaller than that of the matrix. It also proves a long fiber (especially visible in stretching towards load direction). A break in the fiber itself does not necessarily mean the failure of the sample, as the load may continue to be transferred by the matrix. This relationship occurs as a result of adding liquid rubbers with highly reactive carboxyl end groups to the matrix, which translates into an increase in the elongation at break, and thus the impact strength of epoxy resins. This rubber forms a dispersed phase bonded to the epoxy matrix which prevents crack propagation in the matrix [34]. However, in the analyzed case, the strength of the matrix was not sufficient.

In this work investigation of the orientation of the fibers combined with the layup heterogeneity, with further consequences for the structure strength has been examined. As a result of that, one can observe considerable differences in the maximum load of stresses applied to the samples. According to Figure 3 maximum stress values for samples, no. 1, 2 and 3 should be approximately two times higher than for samples no. 4, 5 and 6. However, these are approximately five times higher (1274.0 MPa, 1280.6 MPa and 1212.3 MPa in comparison to 246.2 MPa, 249.1 MPa and 258.7 MPa), while compared to samples 7, 8 and 9 (667.2 MPa, 685.5 MPa and 792.4 MPa) they are almost twice as high.

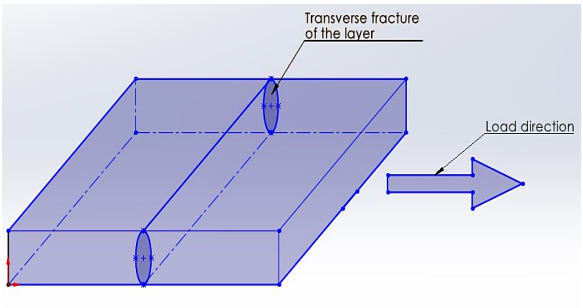

Fig. 21. Crack with transverse stretching of the composite layer

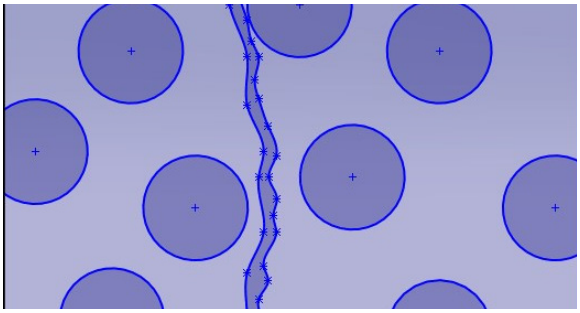

Fig. 22. Crack with transverse stretching of the composite layer in microscale

A similar relationship exists between samples 9–18. This indicates a source independent of the material itself or the lamination technology, and the behavior of fiber-reinforced composite materials, where the fibers break heterogeneously, transferring energy to the next layers.

The materials themselves have similar characteristics, so the results of the strength tests should oscillate at a similar level. However, the structural discontinuities together with air bubbles observed on a microscopic scale contribute to the weakening of individual layers and, consequently, the entire structure. The stresses can be distributed very heterogeneously, which is shown in Figures 10 and 11, so their maxima are not at the ends of the tested samples, nor in the middle section. In Figure 8 stresses are distributed equally over the entire surface of the sample. In Figure 9 stresses tend to be higher in the middle section, where the crack occurs.

The sample rupture moment occurs when all layers are broken. It should be done simultaneously if they are made of the same reinforcement material and in the same matrix. The propagation of the stresses advancing deep into the material is visible in the microstructure of the sample - Figure 18 - where the deformation of the mesh of fibers can be seen, manifested by a change in the directionality of some of them. Importantly, for the pre-impregnated technology (Fig. 17) there are no cracks inside the material – these are only observed at the point where the sample is broken. Therefore, it is the propagation of deformation, but not the propagation of cracks.

CONCLUSIONS

The research showed interesting relationships inside the structure of composite made of carbon fibers in a polymer matrix, which allow the transfer of some loads to other layers of the laminate, which may be used in the creation of such structures. This relationship, however, needs to be better known and understood - whether it is created in a more stochastic or organized manner. The study of the fracture mechanics of composite materials should be carried out by observing the behavior of components on the macroscale and then related to the probable phenomena occurring on the microscale.

The technology of pre-impregnated combination of fibers and uncured resin, activated by the temperature, is characterized by a much better quality of the produced samples, greater repeatability of test results, better strength parameters and fewer technological defects. For the hand lay-up technology the heterogeneous distribution of stresses during the tensile test was very noticeable.

Composites are a group of materials that gives a wide range of properties desired by the engineer at the stage of product creation, because the intended properties of the structure can be obtained by appropriate selection of the matrix material, fibers, their thickness, proportions, and spatial arrangement. However, such structures are characterized by the complexity of the destruction mechanisms. For the tested laminated samples, a gradual, stochastic development of the degradation of the composite structure was noticed, which has its source in local microdamages, microcracks, which then leads to the destruction of the entire structure as the load increases.

When analyzing the stress-strain diagrams, it can be noticed that the samples in which the load was applied along the axis of the fibers behave like an elastic material. Specimens, where the force is applied at an angle to the axis of the fibers, tend to behave like an elastic-plastic material. Materials in which the fibers are arranged at an angle of 45° to the load show much lower strength properties, however, the deformation to the point of failure is much greater.

As a result of the sub-critical crack growth within the resin matrix material the defects are subject to a complex, multi-axial stress field on the micro-scale even if the globally applied force is axial**.**

Fiber breakage does not necessarily results in the failure of the whole composite, as the load may continue to be transferred by the matrix. It is related to adding liquid rubbers with highly reactive carboxyl end groups to the matrix, which translates into an increase in the elongation at break, and thus the impact strength of epoxy resins.

CT scan results show the behavior of composites in the field of fracture mechanics. The propagation of deformations into the material is visible. In case of both lamination technologies it can be seen that the structure of the outermost layer has undergone significant deformation, where the thread has undergone a wavy effect due to the tensile force. An interesting phenomenon of the propagation of deformations and cracks

into the material has been noticed. In case of the pre-impregnated laminate, it can be observed that the structure is deformed into the material, but the layers did not separate from each other. In case of the hand lay-up laminate, a more stochastic delamination of individual layers may be noticed. This indicates mutual protection of the entire structure while subjecting it to the loads.

Correlation of the results of strength tests with the imaging methods made it possible to determine the effect of fiber orientation and structural discontinuities on the overall strength of the composite and its behavior in the area of fracture mechanics. The next step will be to carry out tests on a larger sample and using other destructive tests, e.g. impact strength, three-point bending.

REFERENCES

Kumaresan M., Sathish S., Karthi N.; Effect of fiber orientation on mechanical properties of sisal fiber reinforced epoxy composites. Journal of Applied Science and Engineering, 2015, 18(3): 289-294. https://doi.org/10.6180/jase.2015.18.3.09

1. Rajak D.K., D.D. Pagar, P.L. Menezes, E. Linul; Fiber-reinforced polymer composites: Manufacturing, properties, and applications. Polymers 2019, 11, 1667; https://doi.org/10.3390/polym11101667
2. Mogilski M., M.Jabłoński, M. Deroszewska, R. Saraczyn, J. Tracz, M. Kowalik and W. Rzadkowski; Investigation of energy absorbed by composite panels with honeycomb aluminum alloy core. Materials 2020, 13, 5807; https://doi.org/10.3390/ma13245807
3. Faulstich de Paiva J.M., S. Mayer, M.C. Rezende; Comparison of tensile strength of different carbon fabric reinforced epoxy composites; Mat. Res. 9(1), 2006; https://doi.org/10.1590/S1516-14392006000100016
4. Dziedzic A. Percolation theory and its application in materials science and microelectronics (Part II – Experiments and numerical simulations). Informacije Midem - Ljubljana, 31(2): 141-152
5. Tezara C., J.P. Siregar, H.Y. Lim, F.A. Fauzi, M.H. Yazdi, L.K. Moey, J.W. Lim; Factors that affect the mechanical properties of kenaf fiber reinforced polymer: A review; Journal of Mechanical Engineering and Sciences, 2016, 10(2): 2159-2175. https://doi.org/10.15282/jmes.10.2.2016.19.0203
6. Kaczmar J., Mayer P., Właściwości i zastosowania włókien węglowych i szklanych. Tworzywa Sztuczne i Chemia, 2008, 6: 52-56.
7. Taj S., M.A. Munawar, S. Khan, Natural fiber-reinforced polymer composites, Proc. Pakistan Acad. Sci. 2007, 44(2):129-144.
8. Al-Mosawe A., R. Al-Mahaidi, Xiao-Ling Zhao, Effect of CFRP properties, on the bond characteristics between steel and CFRP laminate under quasi-static loading, Construction and Building Materials, 98, November 2015: 489-501
9. Mulaan N.A., A.S. Mahmood, S. Basturk; The effect of different number of layers and fiber distribution on the performance of composite laminates; Journal of Physics: Conference Series 1973 (2021) 012067; https://doi.org/10.1088/1742-6596/1973/1/012067
10. Chukov D., Nematulloev S., Zadorozhnyy M., Tcherdyntsev V., Stepashkin A., Zherebtsov D.; Structure, mechanical and thermal properties of polyphenylene sulfide and polysulfone impregnated carbon fiber composites; Polymers 2019, 11, 684; https://doi.org/10.3390/polym11040684
11. Giorgini L., L. Mazzocchetti, G. Minak, E. Dolcini; investigation of a carbon fiber/epoxy prepreg curing behavior for thick composite materials production: an industrial case-study. 6th International Conference on Times of Polymers (TOP) and Composites AIP Conf. Proc. 2012, 1459: 190-192. https://doi.org/10.1063/1.4738439
12. Sharma A.P., S.H. Khan, R. Velmurugan; Effect of through thickness separation of fiber orientation on low velocity impact response of thin composite laminates; Article in Heliyon, November 2019; https://doi.org/10.1016/j.heliyon.2019.e02706
13. Kakur N., S. Krishnapillai, V. Ramachandran; Effect of fiber orientation on carbon/epoxy and glass/epoxy composites subjected to shear and bending. Diffusion and Defect Data Pt. B: Solid State Phenomena 267: 103-108; https://doi.org/10.4028/www.scientific.net/SSP.267.103
14. Vasudevan A., S. Senthil Kumaran, K. Naresh, R. Velmurugan, K. Shankar; Advanced 3D and 2D damage assessment of low velocity impact response of glass and Kevlar fiber reinforced epoxy hybrid composites; https://doi.org/10.1080/2374068X.2018.1465310
15. Valot E., P. Vannucci. Some exact solutions for fully orthotropic laminates. Composite Structures, 69(2), July 2005: 157-166; https://doi.org/10.1016/j.compstruct.2004.06.007
16. Boczkowska A., G. Krzesiński; Kompozyty i techniki ich wytwarzania; Oficyna Wydawnicza Politechniki Warszawskiej, Pages: 58-61 and 192-197
17. Do Sy; Material and Application Report 2015 Acrylonitrile Butadiene Styrene (ABS) and 3D Printer (2); https://www.researchgate.net/publication/332538226_Material_and_Application_Report_2015_Acrylonitrile_Butadiene_Styrene_ABS_and_3D_Printer_2 (Accessed on 3.09.2022)
18. Velgosová O., S. Nagy, M. Besterci, V. Puchý; Microstructure and fracture mechanism of Cu-Y2O3

composite; Kovove Mater. 58 2020 363-369; https://doi.org/10.4149/km_2020_5_363

19. Korniejenko K., B. Figiela, C. Ziejewska, J. Marczyk, P. Bazan, M. Hebda, M. Choińska and Wei-Ting Lin; Fracture behavior of long fiber reinforced geopolymer composites at different operating temperatures. Materials, 15(2); https://doi.org/10.3390/ma15020482
20. https://www.astm.org/d3878-20b.html
21. https://www.astm.org/d3039_d3039m-08.html
22. XC110 210g 2x2 Twill 3k prepreg carbon fibre manufactured by Easy Composites Ltd, Stoke-on-Trent, UK. 2020. Available online: https://www.easycomposites.co.uk/xc110-210g-22-twill-3k-prepreg-carbon-fibre (accessed on 2.08.2022)
23. Ahmad F., M. Al Awadh , M. Abas , S. Noor and A. Hameed; Optimization of carbon fiber reinforced plastic curing parameters for aerospace application. Applied Sciences 2022, 12, 4307, https://doi.org/10.3390/app12094307
24. Instron 8516 Fatigue Testing Machine Manufactured by Instron Worldwide, Norwood, MA, USA. Available online: https://www.instron.us/products/testing-systems/dynamic-and-fatigue-systems (accessed on 02.03.2022)
25. Sherif G., Chukov D., Tcherdyntsev V., Torokhov V.; Effect of formation route on the mechanical properties of the polyethersulfone composites reinforced with glass fibers; Polymers 2019, 11, 1364; doi:10.3390/polym11081364
26. Bach H. Application of ion sputtering in preparing glasses and their surface layers for electron microscope investigations. Journal of Non-Crystalline Solids, 3, (1), 1970: 1-32; https://doi.org/10.1016/0022-3093(70)90102-X
27. Das Murtey M. and Ramasamy P. Sample preparations for scanning electron microscopy – life sciences. Modern Electron Microscopy in Physical and Life Sciences, Chapter 8: 161-183
28. Garcea S.C., Y. Wang, P.J. Withers; X-ray computed tomography of polymer composites; Composites Science and Technology, 2018, 156: 305-319; https://doi.org/10.1016/j.compscitech.2017.10.023
29. Zhishen Wu, Xin Wang, Kentaro Iwashita, Takeshi Sasaki, Yasumasa Hamaguchi; Tensile fatigue behaviour of FRP and hybrid FRP sheets; Composites Part B: Engineering, 2010, 41(5): 396-402; https://doi.org/10.1016/j.compositesb.2010.02.001
30. Pansart S. Prepreg processing of advanced fibre-reinforced polymer (FRP) composites; Woodhead Publishing Series in Civil and Structural Engineering 2013: 125-154; https://doi.org/10.1533/9780857098641.2.125
31. Stelzer S., R. Jones, A.J. Brunner; Interlaminar fatigue crack growth in carbon fiber reinforced composites; 19th International Conference on Composite Materials (ICCM19); July 2013
32. Savage G. Sub-critical crack growth in highly stressed Formula 1 race car composite suspension components; Engineering Failure Analysis; https://doi.org/10.1016/j.engfailanal.2008.02.016
33. Fiore V., Valenza A., Epoxy resins as a matrix material in advanced fiber-reinforced polymer (FRP) composites; Woodhead Publishing Series in Civil and Structural Engineering 2013: 88-121; https://doi.org/10.1533/9780857098641.1.88